Delft University of Technology

Back-contacted BaSi$_2$ solar cells

An optical study

Vismara, Robin; Isabella, Olindo; Zeman, Miro

Important note
To cite this publication, please use the final published version (if applicable).
Please check the document version above.

Back-contacted BaSi$_2$ solar cells: an optical study

ROBIN VISMARA,[*] OLINDO ISABELLA, AND MIRO ZEMAN

Delft University of Technology, Photovoltaic Materials and Devices, Mekelweg 4, 2628CD Delft, The Netherlands

[*]*r.vismara@tudelft.nl*

Abstract: We present the optical investigation of a novel back-contacted architecture for solar cells based on a thin barium (di)silicide (BaSi$_2$) absorber. First, through the analysis of absorption limits of different semiconducting materials, we show the potential of BaSi$_2$ for photovoltaic applications. Then, the proposed back contacted BaSi$_2$ solar cell design is investigated and optimized. An implied photocurrent density of 40.3 mA/cm^2 in a 1-μm thick absorber was achieved, paving the way for novel BaSi$_2$-based thin-film solar cells.

References and links

1. ©Fraunhofer ISE: Photovoltaics Report, updated: 17 November 2016.
2. M. A. Green, K. Emery, Y. Hishikawa, W. Warta, and E. D. Dunlop, "Solar cell efficiency tables (version 48)," Prog. Photovolt. Res. Appl. **24**(7), 905–913 (2016).
3. K. Morita, Y. Inomata, and T. Suemasu, "Optical and electrical properties of semiconducting BaSi$_2$ thin films on Si substrates grown by molecular beam epitaxy," Thin Solid Films **508**(1–2), 363–366 (2006).
4. D. B. Migas, V. L. Shaposhnikov, and V. E. Borisenko, "Isostructural BaSi$_2$, BaGe$_2$ and SrGe$_2$: electronic and optical properties," Phys. Status Solidi **244**(7), 2611–2618 (2007).
5. S. Kishino, T. Imai, T. Iida, Y. Nakaishi, M. Shinada, Y. Takanashi, and N. Hamada, "Electronic and optical properties of bulk crystals of semiconducting orthorhombic BaSi$_2$ prepared by the vertical Bridgman method," J. Alloys Compd. **428**(1–2), 22–27 (2007).
6. K. Toh, T. Saito, and T. Suemasu, "Optical absorption properties of BaSi$_2$ epitaxial films grown on a transparent silicon-on-insulator substrate using molecular beam epitaxy," Jpn. J. Appl. Phys. **50**(6R), 068001 (2011).
7. N. A. A. Latiff, T. Yoneyama, T. Shibutami, K. Matsumaru, K. Toko, and T. Suemasu, "Fabrication and characterization of polycrystalline BaSi$_2$ by RF sputtering," Phys. Status Solidi., C Curr. Top. Solid State Phys. **10**(12), 1759–1761 (2013).
8. M. Kumar, N. Umezawa, and M. Imai, "BaSi$_2$ as a promising low-cost, earth-abundant material with large optical activity for thin-film solar cells: A hybrid density functional study," Appl. Phys. Express **7**(7), 071203 (2014).
9. K. O. Hara, Y. Nakagawa, T. Suemasu, and N. Usami, "Simple vacuum evaporation route to BaSi$_2$ thin films for solar cell applications," Procedia Eng. **141**, 27–31 (2016).
10. R. Vismara, O. Isabella, and M. Zeman, "Organometallic Halide Perovskite/Barium Di-Silicide Thin-Film Double-Junction Solar Cells," Proc. SPIE **9898**, 98980J (2016).
11. M. Baba, K. Toh, K. Toko, N. Sato, N. Yoshizawa, K. Jiptner, T. Sekiguchi, K. O. Hara, N. Usami, and T. Suemasu, "Investigation of grain boundaries in BaSi$_2$ epitaxial films on Si(111) substrates using transmission electron microscopy and electron-beam-induced current technique," J. Cryst. Growth **348**(1), 75–79 (2012).
12. M. Baba, K. Ito, W. Du, T. Sanai, K. Okamoto, K. Toko, S. Ueda, Y. Imai, A. Kimura, and T. Suemasu, "Hard x-ray photoelectron spectroscopy study on valence band structure of semiconducting BaSi2," J. Appl. Phys. **114**(12), 123702 (2013).
13. K. O. Hara, N. Usami, K. Nakamura, R. Takabe, M. Baba, K. Toko, and T. Suemasu, "Determination of bulk minority-carrier lifetime in BaSi$_2$ earth-abundant absorber films by utilizing a drastic enhancement of carrier lifetime by post-growth annealing," Appl. Phys. Express **6**(11), 112302 (2013).
14. USGS, "Rare earth elements-Critical resources for high technology," http://pubs.usgs.gov/fs/2002/fs087-02/.
15. ANSYS white paper, "ANSYS HFSS," http://www.ansys.com/Products/Electronics/ANSYS-HFSS.
16. O. Isabella, S. Solntsev, D. Caratelli, and M. Zeman, "3-D optical modeling of thin-film silicon solar cells on diffraction gratings," Prog. Photovolt. Res. Appl. **21**(1), 94–108 (2013).
17. M. Zeman, O. Isabella, S. Solntsev, and K. Jäger, "Modelling of thin-film silicon solar cells," Sol. Energy Mater. Sol. Cells **119**, 94–111 (2013).

18. O. Isabella, H. Sai, M. Kondo, and M. Zeman, "Full-wave optoelectrical modeling of optimized flattened light scattering substrate for high efficiency thin-film silicon solar cells," Prog. Photovolt. Res. Appl. **22**(6), 671–689 (2014).
19. C. Onwudinanti, R. Vismara, O. Isabella, L. Grenet, F. Emieux, and M. Zeman, "Advanced light management based on periodic textures for $Cu(In,Ga)Se_2$ thin-film solar cells," Opt. Express **24**(6), A693–A707 (2016).
20. NREL, "Reference solar spectral irradiance: air mass 1.5," http://rredc.nrel.gov/solar/spectra/am1.5/.
21. M. A. Green, "Lambertian light trapping in textured solar cells and light-emitting diodes: analytical solutions," Prog. Photovolt. Res. Appl. **10**(4), 235–241 (2002).
22. T. Tiedje, E. Yablonovitch, G. D. Cody, and B. G. Brooks, "Limiting efficiency of silicon solar cells," IEEE Trans. Electron Dev. **31**(5), 711–716 (1984).
23. Z. Yu, A. Raman, and S. Fan, "Fundamental limit of light trapping in grating structures," Opt. Express **18**(S3 Suppl 3), A366–A380 (2010).
24. W. Shockley and H. J. Queisser, "Detailed balance limit of efficiency of *p-n* junction solar cells," J. Appl. Phys. **32**(3), 510–519 (1961).
25. Z. Yu, M. Leilaeioun, and Z. Holman, "Selecting tandem partners for silicon solar cells," Nat. Energ. **1**(11), 16137 (2016).
26. K. X. Wang, Z. Yu, V. Liu, Y. Cui, and S. Fan, "Absorption enhancement in ultrathin crystalline silicon solar cells with antireflection and light-trapping nanocone gratings," Nano Lett. **12**(3), 1616–1619 (2012).
27. O. Isabella, A. Ingenito, D. Linssen, and M. Zeman, "Front/rear decoupled texturing in refractive and diffractive regimes for ultra-thin silicon-based solar cells," in *OSA Technical Digest* (2013), paper PM4C.2.
28. S. Yachi, R. Takabe, H. Takeuchi, K. Toko, and T. Suemasu, "Effect of amorphous Si capping layer on the hole transport properties of $BaSi_2$ and improved conversion efficiency approaching 10% in $p-BaSi_2/n$-Si solar cells," Appl. Phys. Lett. **109**(7), 072103 (2016).
29. B. Hoex, S. B. S. Heil, E. Langereis, M. C. M. van de Sanden, and W. M. M. Kessels, "Ultralow surface recombination of *c*-Si substrates passivated by plasma-assisted atomic layer deposited Al_2O_3," Appl. Phys. Lett. **89**(4), 042112 (2006).
30. H. Tan, P. Babal, M. Zeman, and A. H. M. Smets, "Wide bandgap p-type nanocrystalline silicon oxide as window layer for high performance thin-film silicon multi-junction solar cells," Sol. Energy Mater. Sol. Cells **132**, 597–605 (2015).
31. V. Demontis, C. Sanna, J. Melskens, R. Santbergen, A. H. M. Smets, A. Damiano, and M. Zeman, "The role of oxide interlayers in back reflector configurations for amorphous silicon solar cells," J. Appl. Phys. **113**(6), 064508 (2013).
32. A. Ingenito, O. Isabella, and M. Zeman, "Experimental demonstration of $4n^2$ classical absorption limit in nanotextured ultrathin solar cells with dielectric omnidirectional back reflector," ACS Photonics **1**(3), 270–278 (2014).
33. A. Ingenito, S. L. Luxembourg, P. Spinelli, J. Liu, J. C. O. Lizcano, A. W. Weeber, O. Isabella, and M. Zeman, "Optimized metal-free back reflectors for high-efficiency open rear c-Si solar cells," IEEE J. Photovolt. **6**(1), 34–40 (2016).

1. Introduction

Recent years have seen the emergence of crystalline silicon (c-Si) as the dominating technology in the photovoltaic (PV) market [1]. Thin-film approaches for terrestrial applications – e.g. CdTe, $Cu(In,Ga)Se_2$ (CIGS) and thin-film silicon – have so far not been able to outperform c-Si devices [2]. For this reason, materials that are high-performing, abundant and low cost attract great attention. One of such materials is barium di-silicide ($BaSi_2$), which exhibits attractive optoelectrical properties, such as high absorptivity [3–10], large carrier mobility values [11–13], a quasi-direct bandgap between 1.1 eV and 1.3 eV [3–8], abundancy and inexpensiveness [14].

In a previously published optical study [10], we showed how single-junction PV devices based on a very thin (~1 μm) $BaSi_2$ absorber can achieve photocurrent density (J_{ph}) values above 40 mA/cm^2, and that the combination of $BaSi_2$ with an organometallic halide perovskite in a 2-terminal double junction architecture can reach conversion efficiencies up to 28%. These results were obtained by applying advanced light management schemes aimed at promoting: (I) broadband in-coupling of incoming radiation and (II) diffraction of red and near infrared (NIR) photons to enhance their chances of being absorbed. One possible issue, with the structure described in [10], is the realization of good top and bottom electric contacts, due to the complex light trapping scheme necessary to attain the excellent optical performance.

Therefore, in this contribution we introduce an alternative $BaSi_2$ solar cell design: a back-contacted architecture, in which hole- and electron-selective contacts are alternated at the

back side of the device. The optical performance of the proposed layout was investigated and optimized, with the goal of maximizing the absorption in the $BaSi_2$ absorber layer.

2. Modeling approach

The performance of the proposed back-contacted $BaSi_2$ solar cell was analyzed by means of rigorous optical modeling. The Ansoft High Frequency Structure Simulator (HFSS) was employed [15], a three-dimensional (3-D) Maxwell equation solver based on the finite element method that allows for the design and simulation of thin-film devices with arbitrarily complex geometries [10,16–19]. The optical performance was assessed in terms of reflectance (R) and absorptance in each layer i of the model (A_i) [16]. The convolution of A_i with the photon flux of the standard AM1.5g spectrum ($\Phi_{AM1.5}(\lambda)$ [20],) results in the implied photocurrent density $J_{ph\text{-}i}$ generated (in the active layer) or lost (in the i-th supporting layer):

$$J_{\text{ph-}i}(\lambda) = -q\int_{300\,\text{nm}}^{1200\,\text{nm}} A_i(\lambda)\Phi_{AM1.5}(\lambda)d\lambda, \qquad (1)$$

where q is the elementary charge. Note that the calculated implied photocurrent density of the absorber layer ($J_{ph\text{-}BaSi2}$) approximates the short-circuit current of a real device, where processes of charge collection are assumed lossless.

Results of simulations need to be compared with a benchmark, which should represent the performance limit achievable by an equivalent ideal structure. To this purpose, the so-called 'Green limit' was employed [21]. The 'Green limit', which extends the validity of the $4n^2$ limit – proposed by Tiedje and Yablonovitch [22] – to the entire spectrum, represents the maximum absorption achievable by a slab of randomly textured material:

$$A_{\text{Green}} = \frac{1-e^{-4\alpha d}}{1-(1-1/n^2)e^{-4\alpha d}} \qquad (2)$$

where α, d and n are the absorption coefficient, thickness and refractive index of $BaSi_2$, respectively. Although Yu $et\ al.$ showed that thin absorber structures with periodic gratings can surpass the $4n^2$, albeit in limited spectrum portions [23], the 'Green limit' can still be considered a meaningful reference to evaluate the quality of different light trapping schemes.

3. Results and discussion

3.1 Optical limit of PV absorber materials

Since Shockley and Queisser outlined the efficiency limit of single-absorber solar cells, which cannot surpass the 31% barrier [24], great interest has been shown into multi-junction solar cells. These devices can reduce spectral mismatch losses and thus outperform their single-junction counterparts [2]. Particular attention has been focused on double-junction (so-called *tandem*) architectures, due to their relative simplicity of manufacturing with respect to structures with three or more junctions. Tandem solar cells can be categorized with respect to how the two junctions are connected [25]. Two-terminal (2T) devices are electrically and mechanically coupled, while four-terminal (4T) architectures are electrically decoupled, and can either be mechanically stacked or not. Depending on the type of tandem solar cell, appropriate materials for both top and bottom active layers need to be chosen. With respect to the optical performance of absorber materials, two key parameters are the bandgap E_g and the product of the wavelength-dependent absorption coefficient $\alpha(\lambda)$ and its thickness d.

Consider the entire standard solar spectrum AM1.5g [20]. Its total power density ($G_{AM1.5}$) can be calculated by convoluting its photon flux $\Phi_{AM1.5}(\lambda)$ with the energy of photons:

$$G_{AM1.5} = \int_0^\infty \Phi_{AM1.5}(\lambda)\frac{hc}{\lambda}d\lambda \approx 1000\ \text{W/m}^2, \qquad (3)$$

where h is Plank's constant and c the speed of light. On the other hand, the maximum power density a single-junction device can generate (G_{SJ}), assuming no recombination of charge carriers, can be calculated as the integral, up to the bandgap wavelength λ_{gap}, of $\Phi_{AM1.5}(\lambda)$ multiplied by the material bandgap energy:

$$G_{SJ}(\lambda_{gap}) = \frac{hc}{\lambda_{gap}} \int_0^{\lambda_{gap}} \Phi_{AM1.5}(\lambda) d\lambda. \qquad (4)$$

It can be clearly observed that G_{SJ} only depends on the material bandgap. In Fig. 1(a) the black curve depicts Eq. (4) in the spectral range of interest for PV applications.

A more precise description of a material optical potential, however, must also include information about its absorptivity. For this reason, Eq. (4) can be corrected by including the maximal absorption A_{Green} calculated with Eq. (2):

$$G_{Green} = \frac{hc}{\lambda_{gap}} \int_0^{\lambda_{gap}} A_{Green}(\lambda) \Phi_{AM1.5}(\lambda) d\lambda, \qquad (5)$$

where A_{Green} is function of λ, since α is function of λ. The difference between $G_{AM1.5}$ and G_{SJ} represents bandgap-related losses (thermalization and non-absorption), while $G_{SJ} - G_{Green}$ indicates losses that can be characterized as 'intrinsic optical losses'. It is apparent that $G_{SJ} = G_{Green}$ if 100% absorption is assumed (i.e. $A_{Green} = 1$). In Fig. 1(a) G_{Green} of $BaSi_2$ and other PV absorber materials is indicated, assuming a layer thickness of 1 μm. It can be observed that for most materials – amorphous Si (a-Si:H), $CH_3NH_3PbI_3$, CdTe and GaAs – $G_{SJ} \approx G_{Green}$, due to their direct bandgap (i.e. $A_{Green} \approx 1$ for photon energies above the material bandgap). On the other hand, $G_{Green} < G_{SJ}$ for materials with indirect bandgap like CIGS and (particularly) c-Si. In fact, the lower absorption coefficient of such materials – especially in the proximity of their bandgap – results in significant 'intrinsic optical losses'. In terms of absolute optical performance, $BaSi_2$ surpasses all other PV absorber materials except CIGS.

In Fig. 1(b) the power density limit and losses of $BaSi_2$ are more clearly represented ($d = 100$ nm), to highlight how low the 'intrinsic optical losses' are, even for such an ultra-thin layer.
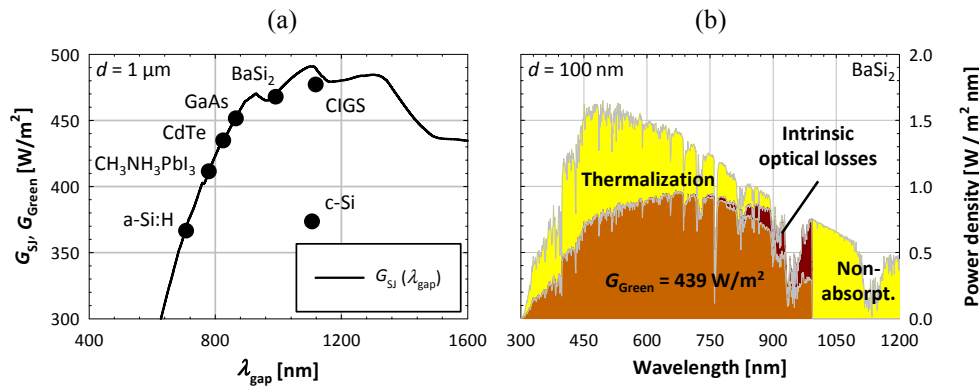

Fig. 1. (a) G_{SJ} (black line) and G_{Green} of 1-μm thick PV materials (black dots). (b) Power density of a 100-nm thick $BaSi_2$ layer, with 'Green limit' and losses indicated.

3.2 Back contact design and optimization

As mentioned earlier, a $BaSi_2$ solar cell architecture, suitable for single-junction and 2T tandem devices, was proposed in a previously published contribution [10]. Such structure, however, relies on the concept of *decoupled texturing* [26], devised to suppress front reflectance and to efficiently scatter red and NIR photons. This type of structure allows thin

slabs of material to achieve very high absorption values [10, 26,27], but could pose severe manufacturing challenges in real devices due to the presence of very tall and steep features.

A back-contacted BaSi$_2$ solar cell is an alternative to the architecture previously proposed. The presence of both hole- and electron-selective contacts at the back side of the device makes this configuration suitable for 4T devices, and allows for complex texturing of the front side where no contacts are located. In this contribution, only the BaSi$_2$ bottom junction is investigated. Possible top-junction solar cells include, among others, amorphous Si and perovskite materials, which thanks to their higher bandgap energy could reduce thermalisation losses with respect to the single-absorber BaSi$_2$ solar cell.
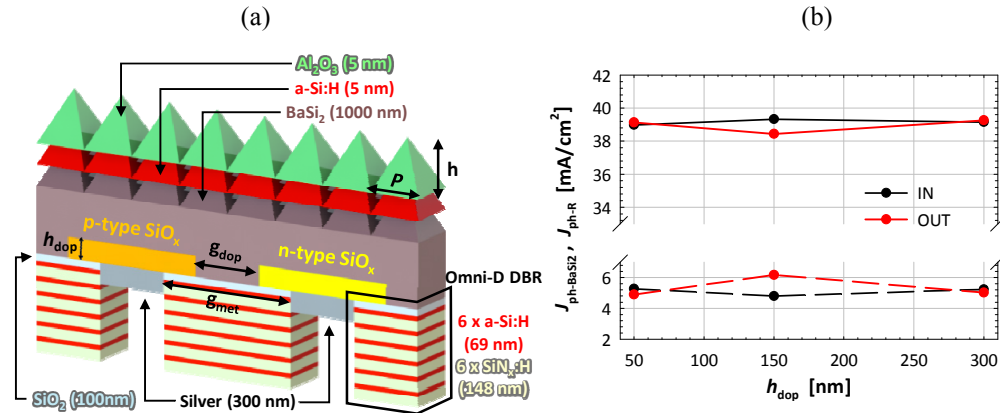

Fig. 2. (a) 3-D sketch of the back-contact BaSi$_2$ solar cell model. (b) Implied J_{ph} generated in the absorber (BaSi$_2$) and lost due to reflection (R), for different values of doping layers height.

A 3D model of the back-contacted BaSi$_2$ solar cell is depicted in Fig. 2(a). At the front side, a series of pyramids with base (P) and height (h) equal to 750 nm is included. This periodic texture reduces the front reflectance of the structure and can scatter light into large angles, promoting its absorption in the BaSi$_2$ layer. Pyramids are coated with two thin (5 nm each) layers of a-Si:H and AlO$_x$, to guarantee the passivation of the top surface [28, 29]. At the back side, fingers of p- and n-doped SiO$_x$ are alternated and contacted with silver, to create hole- and electron-selective contacts, respectively. Such doped materials are chosen for their relatively large bandgap (E_g ~2 eV), ensuring transparency at long wavelengths [30, 31], and for their good thermal stability. The gaps between metallic stripes is covered with a distributed Bragg reflector (DBR), significantly reducing transmittance losses which would otherwise take place. The DBR consists of 6 alternating pairs of a-Si:H (69 nm) and SiN$_x$ (146 nm), making the structure highly reflective around a Bragg wavelength (λ_{Bragg}) of 1000 nm. A 100 nm-thick SiO$_2$ spacer was positioned between absorber and DBR, to improve the reflectance of the back side [32, 33]. The thickness of the BaSi$_2$ layer was fixed to 1 μm, which has demonstrated sufficient to achieve $J_{ph-BaSi2}$ values above 40 mA/cm^2 [10].

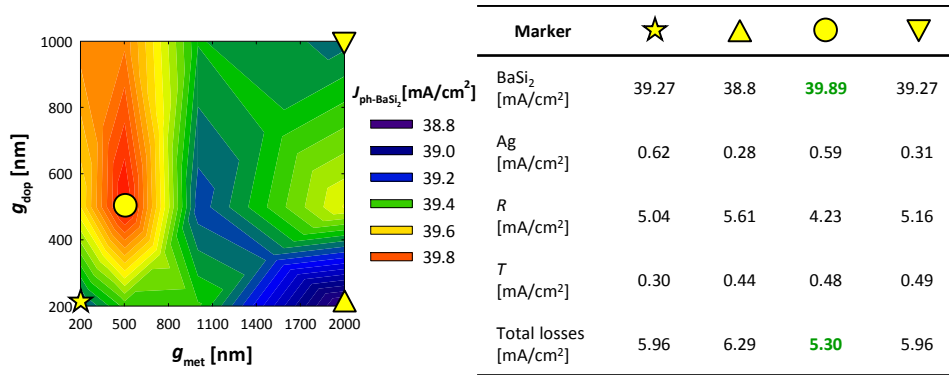| Marker	☆	△	○	▽
BaSi$_2$ [mA/cm²]	39.27	38.8	**39.89**	39.27
Ag [mA/cm²]	0.62	0.28	0.59	0.31
R [mA/cm²]	5.04	5.61	4.23	5.16
T [mA/cm²]	0.30	0.44	0.48	0.49
Total losses [mA/cm²]	5.96	6.29	**5.30**	5.96

Fig. 3. $J_{ph\text{-}BaSi2}$ for different values of distance between doped fingers and between metal contacts (left) and breakdown of J_{ph} absorbed and lost for significant gap distances (right).

The structure was optimized to achieve the best optical performance. The position, size and distance between hole- and electron-selective contacts were investigated. (I) Two possible positions of the doped layers are possible: one where the fingers are within the absorber (*IN*), the other where they are simply deposited on top of BaSi$_2$ layer (*OUT*). (II) The thickness of doped layers (h_{dop}) was varied between 50 nm and 300 nm, for both *IN* and *OUT* configurations. Results, depicted in Fig. 2(b), show that there is small difference between *IN* and *OUT* fingers. In addition, h_{dop} also appears to have little effect on the device optical performance. *IN* configuration with h_{dop} = 150 nm could achieve a slightly higher implied photocurrent than the other possibilities ($J_{ph\text{-}BaSi2}$ = 39.2 mA/cm^2), and was thus selected. (III) The distance between doping layers (g_{dop}) and silver fingers (g_{met}) can also have an impact of the model performance. In this respect, g_{dop} was changed between 200 nm and 1000 nm, while g_{met} between 200 nm and 2000 nm. Results, presented in Fig. 3, show that smaller values of g_{met} (larger metal area) result in larger parasitic losses in the silver contacts. On the other hand, larger gaps between metallic fingers increase transmittance losses. Ultimately, an optimum is found for $g_{dop} = g_{met}$ = 500 nm, for which the sum of parasitic losses in the metallic back contact and the transmittance losses through the DBR is minimized. An implied photocurrent density value of 39.9 mA/cm^2 was achieved.

3.3 Anti-reflective front texture

In Fig. 4(a) reflection and absorption in each layer of the structure are shown. It can be observed that: (i) light in-coupling is not ideal, since reflectance is significant even in the region where BaSi$_2$ is a strong absorber (300 nm – 900 nm); (ii) The passivating a-Si:H layer parasitically absorbs a substantial amount of light in the short wavelength part of the spectrum (300 nm – 600 nm). Light in-coupling can be improved by using taller and steeper pyramids at the front side, while the parasitic absorption of passivating layer can be reduced by employing more transparent materials. Thus, a new structure was modelled, keeping the same period (P = 750 nm) but with taller pyramids (h increased from 750 nm to 875 nm) and coated with a 40-nm thick silicon nitride (SiN$_x$). Result, depicted in Fig. 4(b), show that reflectance and parasitic absorption at the front side are significantly reduced. The $J_{ph\text{-}BaSi2}$ of the new structure increases by 0.4 mA/cm^2 to 40.3 mA/cm^2, a value very close to the best front / back contacted 1-μm thick structure modelled in our previous publication [10].
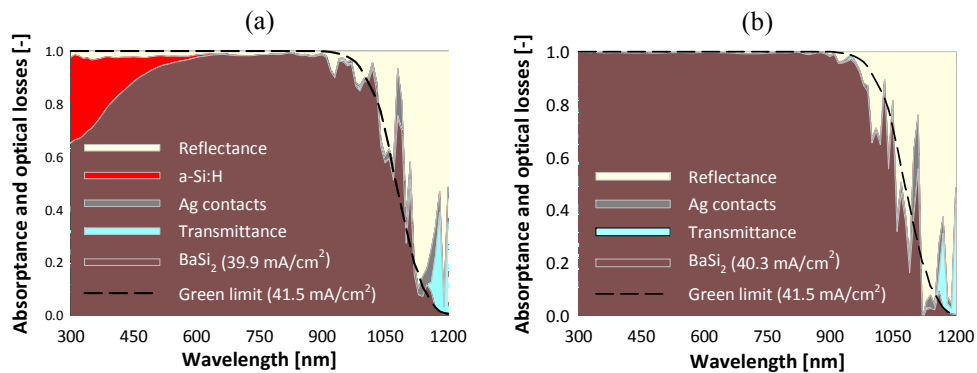
Fig. 4. Absorptance in BaSi$_2$ and optical losses for an architecture with Al$_2$O$_3$ + a-Si:H passivation (a) and with a 40 nm-thick SiN$_x$ passivation (b).

4. Conclusions

BaSi$_2$ is a material that shows great potential for PV applications. In particular, its bandgap makes it a good bottom cell candidate in thin-film tandem devices. The proposed back contacted BaSi$_2$ solar cell is an ideal structure for four-terminal configurations, and the presence of both contacts at the rear side of the device allows the use of advanced light-trapping schemes at the front. After the optimization of doped layers, metal fingers and front texture, an implied photocurrent density of 40.3 mA/cm^2 was achieved. Such a high value, achieved in a configuration with a thin (1 μm) active layer, highlights once again the great potential of BaSi$_2$ as novel absorber for future generation solar cells. Furthermore, the particular configuration of the proposed architecture opens the possibility for the integration of BaSi$_2$ solar cells into 4-terminal tandem devices as bottom junction cell.